UC San Diego
UC San Diego Previously Published Works

Title
The Influence of Nuclear Composition on the Electron Fraction in the Post-Core Bounce Supernova Environment

Permalink
https://escholarship.org/uc/item/5g57k9j8

Journal
The Astrophysical Journal, 472(2)

ISSN
0004-637X

Authors
McLaughlin, Gail C
Fuller, George M
Wilson, James R

Publication Date
1996-12-01

DOI
10.1086/178077

Peer reviewed

THE INFLUENCE OF NUCLEAR COMPOSITION ON THE ELECTRON FRACTION IN THE POST–CORE BOUNCE SUPERNOVA ENVIRONMENT

Gail C. McLaughlin[1] and George M. Fuller[2]
Department of Physics, University of California, San Diego, La Jolla, CA 92093-0319

AND

James R. Wilson
Physical Science Directorate L-140, Lawrence Livermore National Laboratory, Livermore, CA 94550

ABSTRACT

We study the early evolution of the electron fraction (or, alternatively, the neutron-to-proton ratio) in the region above the hot proto–neutron star formed after a supernova explosion. We study the way in which the electron fraction in this environment is set by a competition between lepton (electron, positron, neutrino, and antineutrino) capture processes on free neutrons and protons and nuclei. Our calculations take explicit account of the effect of nuclear composition changes, such as formation of alpha particles (the "alpha effect") and the shifting of nuclear abundances in nuclear statistical equilibrium associated with cooling in near-adiabatic outflow. We take detailed account of the process of weak interaction freezeout in conjunction with these nuclear composition changes. Our detailed treatment shows that the alpha effect can cause significant increases in the electron fraction, while neutrino and antineutrino capture on heavy nuclei tends to have a buffering effect on this quantity. We also examine the effect on weak rates and the electron fraction of fluctuations in time in the neutrino and antineutrino energy spectra arising from hydrodynamic waves. Our analysis is guided by the Wilson and Mayle supernova code numerical results for the neutrino energy spectra and density and velocity profiles.

Subject headings: elementary particles — nuclear reactions, nucleosynthesis, abundances — stars: interiors — supernovae: general

1. INTRODUCTION

In this paper we examine the early evolution of the electron fraction, Y_e, in the post–core bounce supernova environment. The electron fraction is defined to be the net number of electrons per baryon:

$$Y_e = (n_{e^-} - n_{e^+})/n_b = 1/(1 + N_n/N_p), \qquad (1)$$

where n_{e^-}, n_{e^+}, and n_b are the proper number densities of electrons, positrons, and baryons, respectively. The latter expression in equation (1) follows from the condition of overall charge neutrality. Here, N_n and N_p are the total proper neutron and proton densities, respectively, so that $n_b = N_n + N_p$ and N_n/N_p is the net neutron-to-proton ratio.

The electron fraction is a crucial determinant of nucleosynthesis produced from neutrino-heated ejecta in models of post–core collapse supernovae (see Woosley & Baron 1992; Meyer et al. 1992; Woosley et al. 1994; Woosley & Hoffman 1992; Qian et al. 1993; Qian & Woosley 1996; Witti, Janka, & Takahashi 1994; Hoffman et al. 1996a, 1996b). We follow the terminology of Fuller et al. (1992), Fuller (1993), and Qian & Fuller (1995) and divide the post–core bounce evolution of the outflowing material above the nascent neutron star into two epochs: (1) the shock-reheating or "p-process" epoch at times post–core bounce $t_{pb} \lesssim 1$ s; and (2) the neutrino-driven wind or "r-process" epoch at $t_{pb} \gtrsim 1$ s.

We expect the shock reheating epoch to be characterized by chaotic outflow (Burrows, Hayes, & Fryxell 1995; Miller, Wilson, & Mayle 1993; Janka & Müller 1995; Herant et al. 1994; Janka & Müller 1996) and rapid heating by neutrino interactions of material behind the shock. Neutrino-heated ejecta originating from this epoch have been suggested to

give rise to the neutron number $N = 50$ peak r-process material (Woosley & Hoffman 1992; Meyer et al. 1992; Woosley et al. 1994) and possibly at least some of the light p-process nuclei such as ^{92}Mo and ^{96}Ru (Fuller & Meyer 1995; Hoffman et al. 1996a). However, in the Woosley et al. (1994) calculations (based on the Wilson and Mayle supernova results), the $N = 50$ r-process nuclides originating in this epoch are grossly overproduced relative to solar system abundances. Two fixes have been proposed for the "$N = 50$ overproduction problem": (1) Fuller & Meyer (1995) invoke a modification of linear rapid outflow, a high neutrino fluence, and the alpha effect to increase Y_e and thereby reduce $N = 50$ overproduction; and (2) Hoffman et al. (1996a) show that as long as the electron fraction at this epoch can be engineered to be $Y_e \gtrsim 0.484$, $N = 50$ overproduction is avoided. As a bonus, both of these fixes concomitantly suggest that some of the light p-nuclei will be synthesized. Hoffman et al. (1996a) find that the light p-nuclei are produced in the correct proportions so long as $0.484 \lesssim Y_e \lesssim 0.488$. This epoch is characterized by relatively low entropy per baryon, $s/k \sim 40$, and relatively higher Y_e compared to the conditions that may obtain at $t_{pb} \gtrsim 1$ s. Note that the Hoffman et al. (1996a) work implies that we may have to compute Y_e to of order 1% accuracy to predict the nucleosynthesis confidently. It could be that this will not be necessary, as the hydrodynamic outflow is phased in just the right way that a given mass element experiences the necessary Y_e regime at the necessary temperature. Only future computations can address this issue. As we will show, for a given outflow model, predicting Y_e histories to 1% accuracy may be next to impossible at this stage, given our crude understanding of neutrino transport and multidimensional hydrodynamic effects (see Herant et al. 1994; Janka & Müller 1996).

[1] gail@bethe.ucsd.edu.
[2] gfuller@ucsd.edu.

By contrast, the later *r*-process epoch is characterized by considerably higher entropy, $s/k \approx 100$–500 (see Qian & Woosley 1996; Meyer et al. 1992) and possibly by a well-ordered, near–steady state outflow resembling a neutrino-driven wind (Duncan, Shapiro, & Wasserman 1986; Meyer et al. 1992; Qian & Woosley 1996). In fact, Woosley et al. (1994) have shown that the bulk of the solar system's *r*-process material with nuclear mass $A \gtrsim 100$ could be synthesized in this epoch. However, considerable controversy surrounds the theoretical modeling of conditions in the "hot bubble" that forms in this regime. Though the Woosley et al. (1994) calculations yield a nearly perfect solar abundance distribution for the heavier *r*-process nuclides, they are based on the very high entropy ($s/k \sim 400$) conditions obtained by the Wilson and Mayle supernova code. Not only have such high entropies been challenged (Qian & Woosley 1996 find $s/k \lesssim 200$), but even if the entropy were $s/k \gtrsim 300$, neutrino neutral current spallation of alpha particles (Meyer 1995) has been shown to result in a drastic and fatal reduction in the neutron-to-seed ratio required for the *r*-process. Though models show the material in the hot bubble to be quite neutron rich, $Y_e \approx 0.4$, Hoffman et al. (1996b) and Meyer, Brown, & Luo (1996) have demonstrated that far lower values of Y_e are necessary to obtain the requisite neutron-to-seed ratio for the *r*-process if the entropy is $s/k \lesssim 200$. At entropies this low, the bad effects of neutrino spallation of alpha particles (Meyer 1995) would be evaded. Hoffman et al. (1996b) discuss the neutron-to-seed ratio and Y_e issues related to this epoch, while Fuller, Qian, & Wilson (1996) and Caldwell, Fuller, & Qian (1996) discuss neutrino flavor mixing schemes that could give lower Y_e values and hence help the *r*-process.

In this paper we perform a complementary study of the evolution of the electron fraction that concentrates on the effects of nuclear composition changes. We focus in particular on the early time, "low" entropy environment of the shock-reheating epoch. In what follows, we concentrate on the weak interaction balance essentially in a single outflowing mass element (i.e., one-dimensional outflow). We employ outflow results from the Wilson and Mayle supernova code to illustrate various effects bearing on Y_e. It should be kept in mind that we are not *predicting* Y_e, as the Wilson and Mayle results may not be representative of the true picture of supernova evolution. For example, multidimensional hydrodynamic effects could effectively cause different mass elements to have different time/thermodynamic histories. Nevertheless, we choose the simplest case (one-dimensional outflow) to elucidate the physics.

In § 2, we present an overview of all of the variables that affect the calculation of the electron fraction. We show explicitly how the various charged current lepton capture processes are important. In § 3, we discuss salient aspects of the electron neutrino and antineutrino capture rates on free nucleons. We explore the difference between using the Wilson and Mayle transport calculation–derived neutrino energy spectra as an example and approximate blackbody spectra. We also discuss the effect on the electron fraction of hydrodynamic wave-induced fluctuations in the neutrino energy spectra. In § 4, we assess the role of electron and positron capture processes on Y_e. In § 5, we examine the "alpha effect" or the tendency of the formation of alpha particles to raise the electron fraction. We discuss the equilibrium and nonequilibrium nature of weak interaction freezeout in § 6, with particular attention to the role of

nuclear composition changes and the role of neutrino capture on heavy nuclei. We give conclusions in § 7.

2. OVERVIEW

The electron fraction, which is defined in equation (1), can be written in the following way:

$$Y_e = \sum_i (Z_i/A_i)X_i = \sum_i Z_i Y_i . \qquad (2)$$

Here we assume overall plasma charge neutrality, so that the sum in equation (2) runs over all nuclear species i with charge Z_i, nuclear mass number A_i, mass fraction X_i, and number abundance relative to baryons $Y_i = X_i/A_i$. Typically, the material is very hot near the surface of the neutron star, where essentially all of the baryons are in free nucleons. As the material flows away from the neutron star, it cools, and alpha particles begin to form. As it flows farther out and cools further, heavier nuclei near the iron peak begin to form. With this rough evolution of abundances with radius and time in mind, we can rewrite equation (2) as

$$Y_e = X_p + X_\alpha/2 + \sum_h (Z_h/A_h)X_h , \qquad (3)$$

where X_p is the mass fraction of free protons, and X_α is the mass fraction of alpha particles, and the summation runs over all nuclear species h heavier than alpha particles. In the conditions common in neutrino-heated outflow, "free" (not inside nuclei) neutrons and protons, alpha particles, and a few iron peak nuclei typically account for most of the baryons.

The charged current weak interactions alter the electron fraction by converting neutrons into protons and vice versa. Most important in the region above the neutron star are neutrino and antineutrino capture on free nucleons and the associated reverse processes:

$$\nu_e + n \leftrightarrow p + e^- ; \qquad (4)$$

$$\bar{\nu}_e + p \leftrightarrow n + e^+ . \qquad (5)$$

However, the processes of electron neutrino and antineutrino capture on heavy nuclei can sometimes be important in determining the overall neutron-to-proton balance (Fuller & Meyer 1995; McLaughlin & Fuller 1995):

$$\nu_e + A(Z, N) \rightarrow A(Z + 1, N - 1) + e^- ; \qquad (6)$$

$$\bar{\nu}_e + A(Z, N) \rightarrow A(Z - 1, N + 1) + e^+ . \qquad (7)$$

In these expressions, A, Z, and N are the total number of nucleons, proton number, and neutron number of the nucleus, respectively. The reverse rates of electron and positron capture on heavy nuclei are generally negligible for the conditions in which these nuclei form. The ratio of neutrons to protons and Y_e in neutrino-heated material flowing away from the neutron star is set by a competition between the rates of the processes in equations (4), (5), (6), and (7) and the overall material expansion rate (or outflow rate). In fact, it has been shown that where the rates of these processes are rapid compared to the outflow rate, a characteristic weak steady state or "chemical equilibrium" obtains (Qian et al. 1993; Qian 1993). The weak freezeout radius is defined to be where the rate of $n \rightleftharpoons p$ interconversion as set by the rates of the processes in equations (4), (5), (6), and (7) falls below the material outflow rate. Though the details are complicated, Y_e at small radius is set principally by the processes in equations (4) and (5), whereas, at larger radius and at later times,

the processes in equations (6) and (7) can also make a contribution.

The rate of change of the electron fraction of an outflowing mass element resulting from weak interactions may be written as follows (this is a generalization of the treatment in Qian et al. 1993):

$$\frac{dY_e}{dt} = v(r)\frac{dY_e}{dr} \approx (\lambda_{\nu_e} + \lambda_{e+})X_n - (\lambda_{\bar{\nu}_e} + \lambda_{e-})X_p$$
$$+ \sum_h \left(\frac{X_h}{A_h}\right)(\lambda_{h\nu_e} + \lambda_{he+} - \lambda_{h\bar{\nu}_e} - \lambda_{he-}), \qquad (8)$$

where $v(r)$ is the radial velocity field above the neutron star, and t is a time development parameter. In equation (8), the sum on h indicates a sum over all heavy nuclei. Here X_n is the mass fraction of free neutrons, while X_h is the appropriate mass fraction of a heavy nucleus with mass number A_h. We define λ_{ν_e} and $\lambda_{\bar{\nu}_e}$ to be the forward rates of the processes in equations (4) and (5), respectively. Similarly, λ_{e-} and λ_{e+} are the reverse rates of these processes, respectively. Finally, $\lambda_{h\nu_e}(\lambda_{he+})$ and $\lambda_{h\bar{\nu}_e}(\lambda_{he-})$ represent the electron neutrino (positron) and antineutrino (electron) capture rates, respectively, on the nucleus with index h. Note that equation (8) contains *all* the effects that bear on Y_e and the neutron-to-proton ratio in a given mass element. Hydrodynamic motion can influence this weak balance via the position of the weak freezeout radius (Qian et al. 1993). The weak freezeout radius is heavily influenced by the velocity field $v(r)$ [more properly, in multidimensional hydrodynamic regimes, we should write $v(r, \theta, \phi, t)$].

Near the neutron star, before the iron peak nuclei form, the last term in equation (8) is zero. The neutrino and antineutrino capture reactions on free nucleons are usually the fastest of the nuclear charged current weak interaction processes. The exception occurs in the region very close to the neutron star, where electron and positron capture on free nucleons become comparable to the corresponding neutrino capture rates. In the region near the neutron star where the electrons are relativistically degenerate, λ_{e-} can be large and can essentially set Y_e to quite low values. By contrast, at late times and/or large radius, the free nucleons become absorbed into nuclei, and the last term in equation (8) becomes larger than or competitive with the other two terms (in this environment, λ_{he+} and λ_{he-} are always small compared to $\lambda_{h\bar{\nu}_e}$ and/or $\lambda_{h\nu_e}$). Here we include no term that is proportional to X_α, since charged current capture rates on alpha particles are too small to influence the electron fraction in the relevant conditions. Note that since $X_n + X_p + X_\alpha + \sum_h X_h = 1$, and X_α may be a nonlinear function of Y_e (see, for example, eq. [30]), equation (8) is in principle nonlinear.

We can give a formal solution to equation (8) in the limit where there are free nucleons and alpha particles only and no heavy nuclei, and where the dependence of X_α on the electron fraction is neglected:

$$Y_e = \left\{ Y_{ei} - \left[\frac{X_\alpha}{2}\frac{(\lambda_{\bar{\nu}} - \lambda_\nu)}{(\lambda_{\bar{\nu}} + \lambda_\nu)} + \frac{\lambda_n}{(\lambda_n + \lambda_p)}\right]_i \right\}$$
$$\times \exp\left[-\int_{t_i}^{t_f}(\lambda_n + \lambda_p)dt\right] + \left[\frac{X_\alpha}{2}\frac{(\lambda_{\bar{\nu}} - \lambda_\nu)}{(\lambda_{\bar{\nu}} + \lambda_\nu)} + \frac{\lambda_n}{(\lambda_p + \lambda_n)}\right]_f$$

$$-\int_{t_i}^{t_f}\frac{d}{dt}\left[\frac{X_\alpha}{2}\frac{(\lambda_{\bar{\nu}} - \lambda_\nu)}{(\lambda_{\bar{\nu}} + \lambda_\nu)} + \frac{\lambda_n}{(\lambda_p + \lambda_n)}\right]$$
$$\times \exp\left[-\int_t^{t_f}(\lambda_n + \lambda_p)dt'\right]dt. \qquad (9)$$

In this expression the initial conditions are denoted by the subscript i, and the final conditions are denoted by the subscript f. Here, $\lambda_n \equiv \lambda_{e+} + \lambda_{\nu_e}$ and $\lambda_p \equiv \lambda_{e-} + \lambda_{\bar{\nu}_e}$ are the total neutron and proton destruction rates, respectively, resulting from weak interaction processes. When the system is in weak equilibrium, the rate of change of the conditions with time or radius in the plasma will be slow compared with the magnitude of the weak rates λ_n and λ_p. The first term in equation (9) will be negligible when weak equilibrium obtains. The second term in this equation will be the value of the electron fraction as the weak equilibrium limit is approached. The exponential factor in the integrand of the last term is very small except for t near t_f. This factor will not be small for integration intervals, $t - t_f = \delta t \sim 1/(\lambda_n + \lambda_p)$. As long as the product of the time derivatives of X_α and $\lambda_n/(\lambda_p + \lambda_n)$ with δt is small, the last term in equation (9) will also be small. This condition is usually satisfied where weak equilibrium obtains and where the alpha-particle mass fraction is only slowly varying with time. If the system is not in weak equilibrium and/or the alpha-particle mass fraction is changing significantly with time, then in principle, all of the terms in equation (9) may be necessary for calculating the electron fraction. In conditions where the electron fraction is rapidly varying during the period of alpha particle formation, then the dependence of X_α on Y_e must be explicitly included in the solution to equation (8). For this reason, we do not employ equation (9) when we consider the effects of nuclear composition changes on Y_e, but rather we employ a full numerical treatment when solving equation (8) in § 6.

If weak equilibrium is established, alpha particles are absent, and if the electron and positron capture rates, λ_{e-} and λ_{e+}, are both zero, then the electron fraction will be

$$Y_e = 1/(1 + \lambda_{\bar{\nu}_e}/\lambda_{\nu_e}) \equiv Y_{e0}. \qquad (10)$$

This will be a reasonable approximation to the true electron faction at about $t_{pb} \approx 1$ s in the region just below where alpha particles form (Qian et al. 1993). We shall use the quantity Y_{e0} as a first estimate of the electron fraction. We discuss computational estimates of Y_{e0} in detail in § 3.

Although Y_{e0} provides a good first estimate of the electron fraction, the electron and positron capture rates on free nucleons can also have some influence. In fact, at a plasma temperature of ~ 2 MeV, the electron and positron capture rates can make a significant contribution in the determination of the electron fraction. If the system is in weak equilibrium and alpha particles are absent, then the electron fraction in this regime of high plasma temperature is more accurately given by

$$Y_e = 1/[1 + (\lambda_{\bar{\nu}_e} + \lambda_{e-})/(\lambda_{e+} + \lambda_{\nu_e})] = (1 + \lambda_p/\lambda_n)^{-1}. \qquad (11)$$

This can be seen from equation (9) above. At such a high plasma temperature, $X_\alpha \approx 0$ usually will be a good approximation for the relevant entropies in the supernova models we consider. The effect of electron and positron capture on Y_e will be discussed in § 4. We generalize this discussion to include the $X_\alpha \neq 0$ case in § 5.

Fuller & Meyer (1995) first pointed out that the mass

fraction of alpha particles can influence Y_e. This effect can be readily gleaned from equation (9). When the alpha mass fraction rises (plasma temperature ~ 0.5 MeV), free nucleons are typically absorbed into alpha particles. Each alpha particle removes an equal number of free protons (two) and free neutrons (two) when it forms. If the outflowing material in the supernova is neutron rich before the alpha-particle formation, then as the alpha-particle mass fraction increases, the residual free nucleon gas will tend to be enriched in neutrons. Since the charged current capture rates on alpha particles are negligible in this situation, the only interactions that change the electron fraction are lepton captures on free nucleons. However, since alpha-particle formation has left mostly free neutrons, the neutrino and positron capture interactions will have the effect of turning some of these "leftover" free neutrons into protons. In turn, this will cause the total electron fraction to rise. We follow Fuller & Meyer (1995) and call this increase in Y_e due to alpha-particle formation and weak interactions the "alpha effect." We give a detailed treatment of this effect in § 5.

Since the material may not be in weak equilibrium at the time of nuclear reaction rate freezeout and nucleosynthesis, it is necessary to examine the effect on the electron fraction of slow freezeout from weak equilibrium. This is done in § 6, where we present the results of a nonequilibrium calculation of Y_e. The influence on Y_e of neutrino captures on heavy nuclei will also be discussed in § 6. As is evident from equation (8), these processes in principle can impact the final value of the electron fraction. Although it will turn out that the material is no longer in weak equilibrium at the time of formation of iron peak nuclei in the models we consider, the neutrino captures on heavy nuclei (plasma temperature ~ 0.3 MeV) still have some influence on Y_e.

3. NEUTRINO AND ANTINEUTRINO CAPTURE RATES ON FREE NUCLEONS

In this section, we compare the relative magnitude and effects on Y_e of λ_{ν_e} and $\lambda_{\bar{\nu}_e}$. For the calculation of these rates we follow the prescription of Fuller & Meyer (1995) and McLaughlin & Fuller (1995). In computing these rates, we first assume a blackbody distribution for the neutrino spectrum, which we normalize by the neutrino luminosity (see Qian & Fuller 1995). In Figure 1 we depict a zero chemical potential blackbody neutrino (ν_e) energy spectrum (*curve without circles*) with average neutrino energy and normalizing luminosity taken from the numerical results of the Wilson and Mayle supernova calculations at $t_{pb} \approx 0.575$ s. Also shown in this figure is the actual neutrino energy spectrum (*circles*) at large radius at $t_{pb} \approx 0.575$ s as given by the detailed transport calculations of Wilson and Mayle. Of course, the *actual* neutrino energy spectra may differ considerably between different models that employ different transport calculations. We here use the Wilson and Mayle results only as an example.

In our calculations of λ_{ν_e} and $\lambda_{\bar{\nu}_e}$, we generally assume that the material is far from the neutron star, so that the distance dependence of the rates is simply $\propto r_7^{-2}$, where r_7 is the distance from the center of the neutron star in units of 10^7 cm. We further assume that the final state electrons are very relativistic, so that the rate may be expressed with Fermi integrals. In evaluating the Fermi integrals for the antineutrino capture rates, we use the approximation $(m_p - m_n - m_e)/T_{\bar{\nu}} \ll 0$, where m_n is the mass of the neutron,
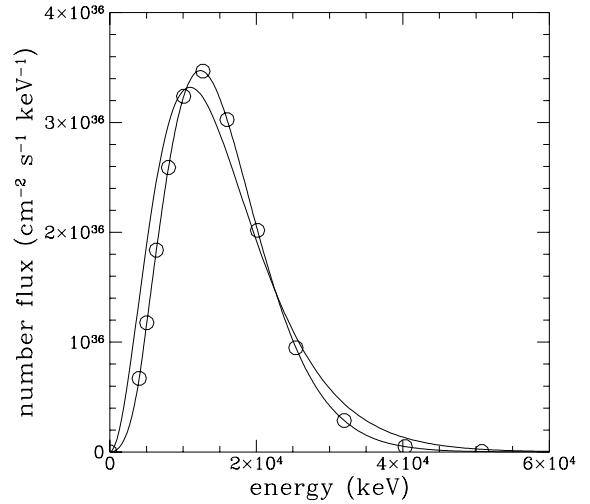

FIG. 1.—Comparison of the Wilson and Mayle numerical transport calculation–derived neutrino energy spectrum with a zero chemical potential blackbody spectrum. Circles indicate the data points taken from the Wilson and Mayle code. The curve through these data points has been fitted using cubic spline interpolation. The curve without circles shows a blackbody spectrum at a temperature of $T_\nu = 3.15$ MeV.

m_p is the mass of the proton, m_e is the mass of the electron, and $T_{\bar{\nu}}$ is the temperature of the antineutrino distribution function (we assume zero chemical potential). The capture rates are then approximately

$$\lambda_{\nu_e} \approx (0.1945 \text{ s}^{-1})\left(\frac{L_\nu}{10^{51} \text{ ergs s}^{-1}}\right)\left(\frac{T_\nu}{\text{MeV}}\right)\left(\frac{1}{r_7^2}\right)C_1; \quad (12)$$

$$\lambda_{\bar{\nu}_e} \approx (0.2000 \text{ s}^{-1}) \exp\left(\frac{-1.804 \text{ MeV}}{T_\nu}\right)$$

$$\times \left(\frac{L_{\bar{\nu}}}{10^{51} \text{ ergs s}^{-1}}\right)\left(\frac{T_{\bar{\nu}}}{\text{MeV}}\right)\left(\frac{1}{r_7^2}\right)C_2 . \quad (13)$$

In this expression we have approximated the initial and final state lepton kinematics as completely relativistic, and we have neglected final state lepton blocking (McLaughlin & Fuller 1995). The terms C_1 and C_2 are defined in the following way:

$$C_1 \approx 1 + (0.6283 \text{ MeV})/T_\nu + (0.1292 \text{ MeV}^2)/T_\nu^2 ; \quad (14)$$

$$C_2 \approx 1 + (1.158 \text{ MeV})/T_{\bar{\nu}}$$

$$+ (0.600 \text{ MeV}^2)/T_{\bar{\nu}}^2 + (0.1778 \text{ MeV}^3)/T_{\bar{\nu}}^3 . \quad (15)$$

These estimates demonstrate the dependence of the rates on neutrino (antineutrino) luminosity, $L_{\nu(\bar{\nu})}$, the temperature, $T_{\nu(\bar{\nu})}$, and distance from the neutron star center, r_7. The rates $\lambda_{\bar{\nu}_e}$ and λ_{ν_e} are approximately proportional to the antineutrino and neutrino temperature, respectively, when these temperatures are large. However, at lower neutrino and antineutrino temperature, they have a more complicated temperature dependence through the terms C_1 and C_2 and the exponential term in equation (13). The exponential term in the antineutrino capture rate has its origin in the energy threshold, $m_n - m_p + m_e$. Of course, there is not a corresponding term in the neutrino capture rate, since neutrino capture on free neutrons has no energy threshold. We estimate the temperature of the blackbody distribution to be $\approx \bar{E}/3.15$, where $\bar{E}$ is the average energy of the neutrino or antineutrino spectrum, as appropriate. At $t_{pb} \approx 0.500$ s, the

neutrino temperature is $T_\nu \approx 3.85$ MeV, and the antineutrino temperature is $T_{\bar\nu} \approx 4.93$ MeV in the Wilson and Mayle numerical calculations.

The ratio of the antineutrino and neutrino capture rates on free nucleons is

$$\frac{\lambda_{\bar\nu_e}}{\lambda_{\nu_e}} \approx 1.029 \left(\frac{L_{\bar\nu}}{L_\nu}\right)\left(\frac{T_{\bar\nu}}{T_\nu}\right) \exp\left[\frac{(-1.804 \text{ MeV})}{T_{\bar\nu}}\right] J_1 , \quad (16)$$

where the term J_1 is defined as

$$J_1 \equiv \left(\frac{C_2}{C_1}\right) \approx 1 + \frac{(1.158 \text{ MeV})}{T_{\bar\nu}} - \frac{(0.6283 \text{ MeV})}{T_\nu} . \quad (17)$$

Since the neutrino and antineutrino temperatures are relatively high, we have ignored terms of higher order in these temperatures in J_1. Because of the neutron excess in the neutron star, $T_{\bar\nu_e}$ will be generally larger than T_{ν_e} everywhere above the neutrino sphere (we ignore possible neutrino flavor mixing effects—see Qian et al. 1993 and Qian & Fuller 1995). Also, at this epoch, the total energy luminosity of the neutrinos is about 10% smaller than that of the antineutrinos in the Wilson and Mayle supernova results. In order for the antineutrino capture rate to dominate over the neutrino capture rate, the antineutrino temperature and luminosity must be sufficiently greater than the corresponding neutrino temperature and luminosity to overcome the effect of the energy threshold. Since the neutrino and antineutrino capture rates have the same dependence on distance from the neutron star, the relative importance of the rates does not change explicitly with radius in this formulation.

The ν_e and $\bar\nu_e$ temperatures and luminosities change with time, and therefore the neutrino and antineutrino capture rates are changing implicitly as the material flows away from the neutron star. The ratio of our approximate antineutrino capture rate on protons to our approximate neutrino capture rate on neutrons has been plotted as a function of time (or epoch) in Figure 2. The antineutrino capture rate is always larger that the neutrino capture rate in the indicated time interval, and this difference is increasing with time. The curve in Figure 2 has been smoothed into a straight line for illustrative purposes. Variations of this ratio from a strictly increasing function will be discussed further below.

Since the ratio $\lambda_{\bar\nu_e}/\lambda_{\nu_e}$ is important for the calculation of the electron fraction, it is better to use the numerically computed energy spectrum to calculate the neutrino and antineutrino capture rates. An example of such a numerically calculated energy spectrum taken from the results of the Wilson and Mayle code is shown in Figure 1. The circles in Figure 1 show the points produced by the detailed neutrino transport computations of this code. In order to calculate the capture rates from these numerical points, it is first necessary to interpolate to find a value of the energy occupation probability for all neutrino energies. Given such an interpolation scheme, the capture rates can be calculated with the expressions

$$\lambda \approx \frac{1 - [1 - (R_{\nu(\bar\nu)}/r)^2]^{1/2}}{1 - [1 - (R_{\nu(\bar\nu)}/r_0)^2]^{1/2}} \int_{E_{TH}}^{\infty} \sigma(E) f_{\nu(\bar\nu)}(E) dE . \quad (18)$$

Here, $f_{\nu(\bar\nu)}(E)$ is the interpolated value for the number flux of (anti)neutrinos at energy E. The (anti)neutrino sphere radius is given by $R_{\nu(\bar\nu)}$, and r is the distance from the neutron star center at which the rate is to be calculated. The distance
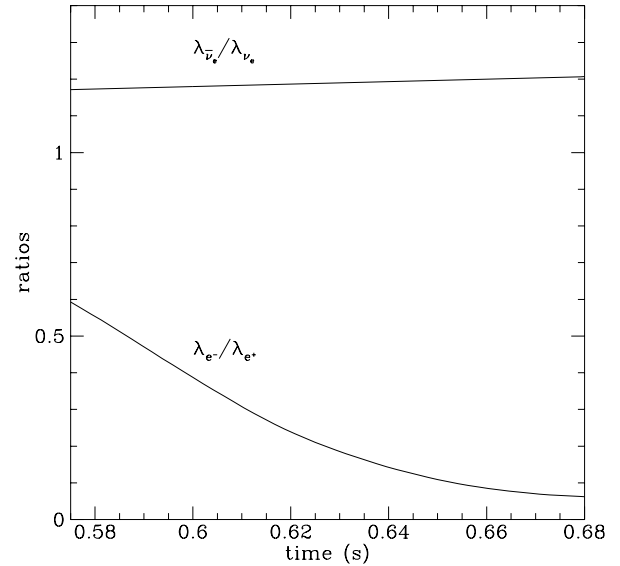

FIG. 2.—Upper curve is the ratio of the neutrino capture rate on free neutrons to the antineutrino capture rate on free protons plotted against time. This curve has been smoothed in order to average out fluctuations in the neutrino spectra. The lower curve is the ratio of the electron capture rate on free protons to the positron capture rate on free neutrons plotted against time, in a mass element moving away from the neutron star.

from the neutron star center at which the neutrino spectrum has been evaluated is r_0. In the case of the Wilson and Mayle code, this distance is $r_0 = 3 \times 10^7$ cm. Assuming relativistic lepton kinematics and no final state lepton blocking, the cross section at energy E is given by

$$\sigma(E) \approx (9.542 \times 10^{-44} \text{ cm}^2)\left(\frac{E + Q}{\text{MeV}}\right)^2 , \quad (19)$$

where Q is the approximate nuclear Q-value (see eq. [4] in McLaughlin & Fuller 1995). The Q-value for neutrino capture on neutrons is $Q \approx 1.293$ MeV, while for antineutrino capture on protons, it is $Q \approx -1.293$ MeV. The energy threshold is $E_{TH} = 0$ for neutrino capture on neutrons, while it is $E_{TH} = (m_n - m_p + m_e) \approx 1.804$ MeV for antineutrino capture on protons.

Table 1 illustrates the discrepancies in capture rates and electron fractions calculated by different methods. In the first column of this table, the method of calculating the neutrino or antineutrino spectrum is given. In the second and third columns, the corresponding neutrino and antineutrino capture rates on free neutrons and protons, respectively, are given. In the fourth column, the quantity $Y_{e_0} = 1/(1 + \lambda_{\bar\nu_e}/\lambda_{\nu_e})$ is tabulated. All rates are calculated at a distance from the neutron star center of $r = 4.793 \times 10^6$ cm. All quantities are calculated at time $t_{pb} = 0.575$ s in the Wilson and Mayle calculations. The $\nu_e(\bar\nu_e)$ temperatures employed for the blackbody spectra in the first row are $T_{\nu_e} = 3.724$ MeV and $T_{\bar\nu_e} = 4.835$ MeV.

TABLE 1

COMPARISON OF THE EFFECTS OF DIFFERENT FITS OF NEUTRINO AND ANTINEUTRINO SPECTRA

Method	λ_{ν_e} (s^{-1})	$\lambda_{\bar\nu_e}$ (s^{-1})	Y_{e_0}
Blackbody spectra	39.10	45.86	0.4602
Cubic spline interpolation........	35.61	38.96	0.4775
Pieces of blackbody spectra......	35.54	38.69	0.4787

The first row of Table 1 shows the results of the calculations with zero chemical potential blackbody neutrino and antineutrino energy spectra. Such a blackbody energy distribution tends to overestimate the (anti)neutrino capture rate. This is because of depletion in the high-energy tail of the actual transport calculation–derived neutrino energy spectrum relative to the zero chemical potential blackbody approximation. This depletion is caused by (anti)neutrino absorption and scattering above the neutrino sphere. The blackbody spectrum tends to underestimate the electron fraction, as shown in the column labeled Y_{e0}.

The second row of Table 1 gives the resulting capture rates and electron fraction when cubic spline interpolation is used to generate the segments of curve between the points on the numerically derived (anti)neutrino energy spectra and equations (18) and (19) are used to calculate the capture rates. In order to check the suitability of this method for our purposes, we tried another interpolation scheme to estimate the capture rates. We fitted curves between the numerically derived spectrum points with pieces of blackbody distribution. The Wilson and Mayle spectrum points themselves are derived from the numerical transport calculations and are produced with an interpolation procedure in some ways similar to that employed here.

Each such blackbody segment had a different temperature. As the neutrinos leave the neutron star, different energy neutrinos decouple at different radii and temperature. This motivated our fitting of the neutrino spectrum by pieces of different thermal distributions. The results are shown in the third row of Table 1. The difference between the approximate electron fraction Y_{e0} obtained in this last case and in the case of cubic spline interpolation was about 0.3%. The difference in Y_{e0} between the case with cubic spline interpolation and the case with a single zero chemical potential blackbody distribution was about 4%. Since it may be necessary to obtain the value of the electron fraction to within 1% (Hoffman et al. 1996a; Qian & Woosley 1996), cubic spline interpolation gives an adequate result. This is the method that we have employed in our calculations of the neutrino and antineutrino capture rates throughout the remainder of this paper.

Figure 3 shows the value of the parameter Y_{e0} at different times, calculated using cubic spline interpolation for the neutrino and antineutrino energy spectra taken from a particular run of the Wilson and Mayle supernova code (crosses). There is significant variation in this quantity during the time increment ($\Delta t \approx 0.025$ s^{-1}) between typical snapshots of the neutrino and antineutrino energy spectra at $t_{pb} \lesssim 0.575$ s. In the hot bubble above the neutrino sphere, hydrodynamical waves are propagating back and forth. Spherical convergence may amplify these waves near the neutrino sphere. Multidimensional nonspherical geometries may complicate this picture considerably (Burrows et al. 1995; Janka & Müller 1995). The variations evident in Figure 3 may be due to these physical effects. The value of Y_{e0} obtained with a similar procedure, but employing a different Wilson and Mayle numerical model for this epoch suggests smaller variations. In any case, since we may need to compute Y_e to of order $\sim 1\%$ accuracy for nucleosynthesis purposes (Hoffman et al. 1996a), it is important to be aware of this issue. Since this variation in Y_{e0} is relatively large ($\sim 3\%$), it will be necessary to resolve this and other issues before the electron fraction can be reliably calculated to accuracies of $\sim 1\%$ during this epoch. It is obvious from
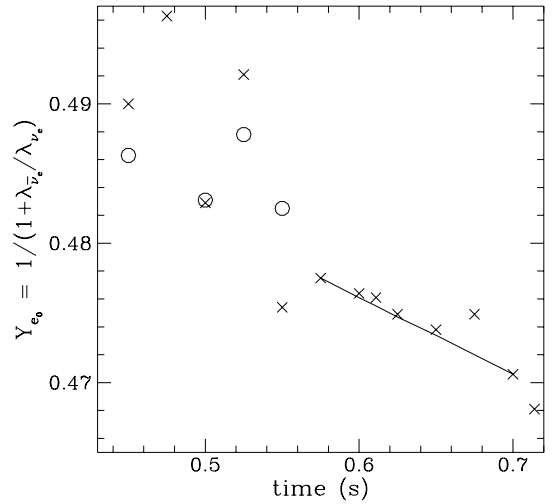

FIG. 3.—Plot of the quantity Y_{e0} against time. The crosses correspond to points calculated from neutrino spectral data taken from the Wilson and Mayle supernova code (crosses). The same quantity derived similarly from a different run of this code is also shown (circles). The line shows the function used in this paper to derive the quantity Y_{e0}.

these considerations that other supernova outflow models, employing different (anti)neutrino energy spectra and/or different hydrodynamic conditions, may well give a Y_e very different from that computed here. Our results are meant to be only illustrative of the physics required to estimate Y_e to 1% for any model.

For illustrative purposes we have chosen to draw a straight line through the time period 0.575–0.700 s (during which the point-to-point variations in Y_{e0} are small), yielding the linear relation

$$Y_{e0} \approx 0.4606 - 0.7120(t - 0.5750) . \qquad (20)$$

This line, which is shown in Figure 3, is meant only to demonstrate the effect of the increasing disparity between the neutrino and antineutrino energy spectra with time on Y_{e0}.

The neutrino and antineutrino energy spectral data that we use here come from snapshots taken from the Wilson and Mayle output at various times post–core bounce. At each time, these spectra have been evaluated at a radius of 3×10^7 cm. However, the neutrino and antineutrino energy spectra will change at different points in the region above the neutron star because of weak interaction processes in the plasma. For the situation we are considering, we are far from the neutrino sphere and close to the radius r_0 of spectral quantity evaluation. However, it is clear that the effects of neutrino emission, absorption, and scattering must also be included for a precise determination of Y_{e0} in the region near the neutron star. We believe that these effects are smaller than the observed oscillation in the quantity Y_{e0} that is apparently caused by local variations from hydrodynamic waves.

4. ELECTRON AND POSITRON CAPTURE RATES ON FREE NUCLEONS

The processes of electron and positron capture on free nucleons are given in equations (4) and (5). These processes are important in regions close to the neutron star. They play a role in determining the position of the gain radius. Neutrino interactions cause a net positive heating of the

region above the gain radius (Bethe & Wilson 1985). At an early epoch ($t_{\rm pb} \lesssim 1$ s), the weak freezeout radius, or distance from the neutron star center at which the characteristic rate of weak interactions becomes smaller than the rate of material outflow in the supernova, occurs sufficiently beyond the gain radius so that electron and positron capture rates on free nucleons have fallen considerably below the corresponding neutrino and antineutrino capture rates. At this distance, and at all points farther away from the neutron star, the electron (positron) capture rates are always much smaller than the (anti)neutrino capture rates on free nucleons.

Here we give estimates of the electron and positron capture rates on free nucleons, analogous to the estimates of neutrino and antineutrino capture rates presented in § 3 (eqs. [12] and [13]). We employ Fermi-Dirac distributions for the electrons and positrons, since these particles are well approximated as being in thermal equilibrium with the plasma. This is a much different situation than the case of neutrinos, since the neutrinos decouple from the plasma very close to the neutron star. In producing these estimates, we have assumed that the electrons are relativistic, so that the appropriate phase space factors may be reduced to Fermi integrals (Fuller, Fowler, & Newman 1985, 1982a, 1982b, 1980; Fuller 1982). Although the electrons and positrons are not completely relativistic throughout the entire period of interest for nucleosynthesis, their capture rates on free nucleons are important only at fairly high temperatures ($T_e > 1$ MeV) and relatively small distances from the neutron star. Therefore, this approximation is sufficient to demonstrate the general effect of these capture rates on the electron fraction. The estimates of the rates are given by

$$\lambda_{e^-} \approx (1.578 \times 10^{-2} \text{ s}^{-1}) \left(\frac{T_e}{m_e c^2} \right)^5$$

$$\times \exp \left(\frac{-1.293 + \mu_{e^-}}{T_e} \right) C_3 ; \qquad (21)$$

$$\lambda_{e^+} \approx (1.578 \times 10^{-2} \text{ s}^{-1}) \left(\frac{T_e}{m_e c^2} \right)^5$$

$$\times \exp \left(\frac{-0.511 - \mu_{e^-}}{T_e} \right) C_4 . \qquad (22)$$

Here C_3 and C_4 are defined in the following way:

$$C_3 \approx 1 + (0.646 \text{ MeV})/T_e + (0.128 \text{ MeV}^2)/T_e^2 ; \quad (23)$$

$$C_4 \approx 1 + (1.16 \text{ MeV})/T_e + (0.601 \text{ MeV}^2)/T_e^2$$

$$+ (0.178 \text{ MeV}^3)/T_e^3 + (0.035 \text{ MeV}^4)/T_e^4 . \quad (24)$$

In these expressions, as everywhere in this paper, the total electron chemical potential μ_{e^-} is defined as the kinetic chemical potential plus the rest mass of the electron. We have estimated the value of the Fermi integrals (see Fuller et al. 1985, eqs. [5a]–[5f]) assuming $(m_p - m_n + \mu_{e^-})/T_e \ll 0$. Clearly, this assumption is valid only when the electrons are not very degenerate. The region we are studying is far from the neutron star and is at sufficiently high temperature and low density that this approximation is reasonable. These rates depend strongly on temperature, which causes their magnitude to fall quickly in the outflowing material. Because of the many approximations involved in obtaining these expressions, they may not faithfully represent the true rates to the accuracy necessary for nucleosynthesis calcu-

lations. Therefore, we use them only to illustrate their influence on the electron fraction. For example, convection or other multidimensional effects could necessitate following the lepton capture rates in degenerate conditions that would modify the evaluation of the rates in equations (21) and (22). The nonequilibrium calculation presented in § 6 includes a more precise calculation of the electron and positron capture rates.

The first question that we address concerns the relative magnitude of these rates. We can combine the approximate expressions for the rates into a ratio:

$$\frac{\lambda_{e^-}}{\lambda_{e^+}} \approx \exp \left[\frac{(-0.782 + 2\mu_{e^-})}{T_e} \right] \left(\frac{C_3}{C_4} \right), \qquad (25)$$

were we intend μ_{e^-} and T_e to be expressed in units of MeV. The reduction in the ratio caused by the threshold for the electron capture reaction is contained in the term $\exp(-0.782 \text{ MeV}/T_e)$. The expression in equation (25) also demonstrates the effect of the chemical potential in reducing the positron capture rate. In general, the temperature in the region of interest is not high enough to neglect the additional multiplicative term, C_3/C_4, which comes from the evaluation of the phase space factors. In Figure 2, we show a plot of this ratio. The curve $\lambda_{e^-}/\lambda_{e^+}$ is depicted starting (far left) in conditions where the system is in weak equilibrium, at a temperature of about $T_e \approx 2$ MeV. This corresponds to a time of $t_{\rm pb} = 0.575$ s in the figure.

In our calculated estimates of $\lambda_{e^-}/\lambda_{e^+}$ in Figure 2, we have utilized an initial Y_e from the weak equilibrium condition, a time-dependent density fit to the Wilson and Mayle supernova computational results, and a constant value of the entropy per baryon set to $s/k = 80$. In an actual supernova we would not expect the entropy of the outflow to be constant, nor would we expect $s/k \approx 80$ to obtain necessarily. We pick $s/k = 80$ and approximate the outflow as adiabatic for illustrative purposes only. In § 6, we consider other values of s/k. Our time-dependent density fit can be taken to represent the density history of an outflowing Lagrangian mass zone during a limited time period. The functional form we have adopted for this fit is

$$\rho \approx \exp (-310.154 + 1811.43t$$

$$- 3215.62t^2 + 1839.84t^3) \text{ g cm}^{-3} , \qquad (26)$$

where t is time in seconds post–core bounce. We have calculated all other thermodynamic variables, such as the temperature and chemical potential, from this density fit and assumed entropy. If the assumed entropy is decreased, then the effect of electron degeneracy will exhibit itself in the ratio of the rates. In this case, the ratio of the electron capture rate to the positron capture rate will be greater than that shown in Figure 2, since the number density of electrons will be enhanced, while the number density of positrons will be suppressed. The ratio $\lambda_{e^-}/\lambda_{e^+}$ decreases at lower temperature (larger time) because of the increasing importance of the threshold for electron capture and also because of the increasing ratio of positron number density to electron number density. It can be seen from this figure that the ratio of the electron capture rate to the positron capture rate exhibits much more variation than the ratio of the antineutrino capture rate to the neutrino capture rate on free nucleons.

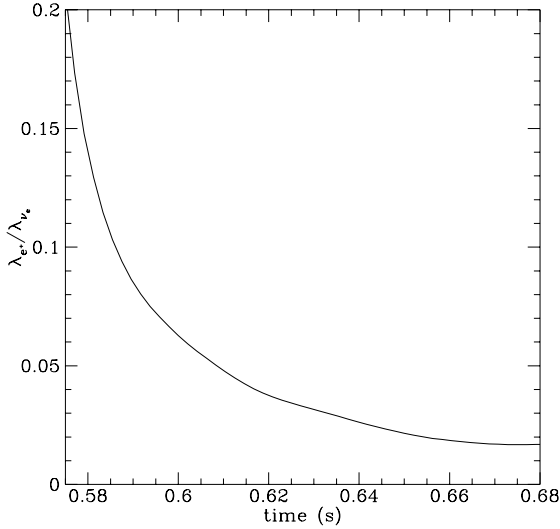The ratio of the positron capture rate to the neutrino capture rate on free nucleons can serve to illustrate an

Fig. 4.—Ratio of the positron capture rate on free neutrons to the neutrino capture rate on free neutrons against time for an outflowing mass element.

important point about the evolution of conditions with radius and time in the outflowing material. The ratios may be expressed as follows:

$$\frac{\lambda_{e+}}{\lambda_{v_e}} \approx 2.34 \left(\frac{T_e}{\text{MeV}}\right)^5 r_7^2 \left(\frac{10^{51}\,\text{ergs}}{L_{v_e}}\right)\left(\frac{\text{MeV}}{T_{v_e}}\right)$$
$$\times \exp\left[\frac{(-m_e - \mu_{e-})}{T_e}\right]\left(\frac{C_4}{C_1}\right), \qquad (27)$$

where the electron rest mass is $m_e \approx 0.511$ MeV. In Figure 4 we plot $\lambda_{e+}/\lambda_{v_e}$ as a function of time. It is evident from this figure that as a mass element flows away from the neutron star, λ_{e+} drops off more quickly than does λ_{v_e}. The drop in
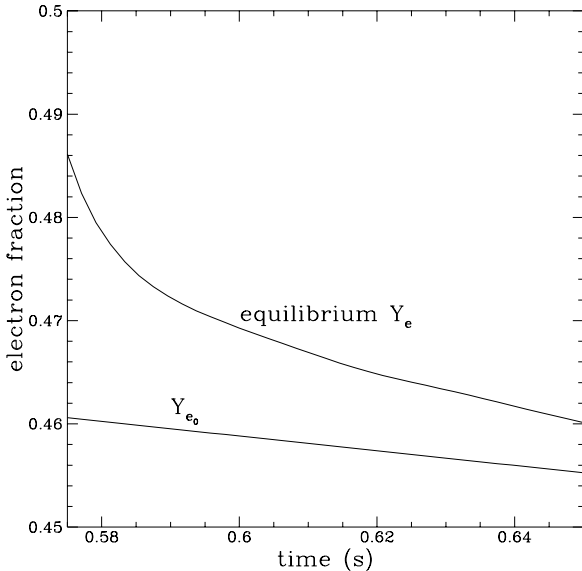

Fig. 5.—Value that the electron fraction of an outflowing mass element would take if the system were in weak equilibrium. The lower curve takes into account only neutrino and antineutrino captures on free nucleons. The upper curve also takes into account electron and positron captures on free nucleons. In calculating these curves, it has been assumed that the nucleons are free at all times and have not been incorporated into nuclei.

λ_{e+} is a result of the rapid decrease in plasma temperature with radius, while the drop in λ_{v_e} with radius simply reflects the relatively slower falloff in the neutrino flux (the $1/r_7^2$ term in eq. [12]). The decrease in the electron chemical potential μ_{e-} with radius has a relatively smaller effect in comparison to the fall in plasma temperature in setting $\lambda_{e+}/\lambda_{v_e}$.

Since, as shown above, the electron and positron capture rates on free nucleons are small relative to the corresponding neutrino and antineutrino capture rates, the electron fraction may be written as an expansion in the small parameter $\lambda_{e+}/\lambda_{v_e}$. Employing this small parameter, we can expand the expression for the electron fraction in equation (9) to yield

$$Y_e \approx Y_{e0}\{1 + (\lambda_{e+}/\lambda_{v_e})[1 - (1 + \lambda_{e-}/\lambda_{e+})/(1 + \lambda_{\bar{v}_e}/\lambda_{v_e})]\}$$
$$+ \mathcal{O}[(\lambda_{e+}/\lambda_{v_e})^2] . \qquad (28)$$

The first-order term in this equation is sufficient to show the effect of electron (positron) capture rates on the "equilibrium" Y_e. Since the lepton capture processes are not necessarily in true chemical or steady state equilibrium, by "equilibrium" Y_e here we mean the Y_e that would obtain if the system were in true equilibrium. As the material flows outward in the region of interest, the term $\lambda_{e+}/\lambda_{v_e}$ decreases rapidly. This term represents the competition between increasing distance from the neutron star and decreasing plasma temperature. However, the term $[1 - (1 + \lambda_{e-}/\lambda_{e+})/(1 + \lambda_{\bar{v}_e}/\lambda_{v_e})]$ actually shows a slight increase with radius or time. This is caused by the decreasing ratio $\lambda_{e-}/\lambda_{e+}$. In the example discussed here, the increase in the term $[1 - (1 + \lambda_{e-}/\lambda_{e+})/(1 + \lambda_{\bar{v}_e}/\lambda_{v_e})]$ is overwhelmed by the decreasing positron capture rate in the leading $\lambda_{e+}/\lambda_{v_e}$ term, so that the change in the "equilibrium" electron fraction with radius is dominated by the behavior of $\lambda_{e+}/\lambda_{v_e}$.

Figure 5 shows this "equilibrium" electron fraction. The upper curve labeled "equilibrium Y_e" includes the effect of electron and positron captures on free nucleons. The lower curve in this figure labeled "Y_{e0}" includes only neutrino captures on free nucleons. At high temperature ($T_e \approx$ 2 MeV) corresponding to early times, the electron and positron captures make a considerable difference in the electron fraction (on the order of $\approx 10\%$). In fact, we have slightly underestimated their effect by using the approximate expressions for the rates in equations (21) and (22). However, it is clear that these processes become less important with time, as the "equilibrium" electron fraction slowly approaches asymptotically the value of Y_{e0}. In more electron degenerate conditions, the electron capture rate may be greater than the positron capture rate, causing the "equilibrium" electron fraction to lie below Y_{e0}. This is the case at early times. In our example, the electron and positron capture processes change the "equilibrium" electron fraction by about 2% just before alpha-particle formation. We emphasize that this conclusion depends on our particular Wilson and Mayle outflow history. Different models will give disparate Y_e values (the results of § 6 for different entropies could be used to gauge how different Y_e might be in other, more realistic models).

5. THE ALPHA EFFECT

In this section we use the "equilibrium" Y_e to discuss qualitatively the behavior of the electron fraction during alpha-particle freezeout. The formation of alpha particles

occurs while the outflowing plasma is still in nuclear statistical equilibrium (NSE). Therefore, the mass fraction of alpha particles at a given density and temperature is well approximated by the Saha equation:

$$X(N, Z) = \frac{G(N, Z)}{\rho N_A} A^{5/2} \left[\frac{2\pi \hbar^2 N_A}{kT_e} \right]^{3(A-1)/2}$$

$$\times \left(\frac{\rho N_A X_n}{A_n} \right)^N \left(\frac{\rho N_A X_p}{A_p} \right)^Z 2^{-A} \exp \left[\frac{Q_n(N, Z)}{kT_e} \right], \quad (29)$$

$$X_\alpha \approx \frac{3.256 \times 10^{-5} \rho_{10}^3}{(T_e/\text{MeV})^{9/2}} X_n^2 X_p^2 \exp \left(\frac{28.29 \text{ MeV}}{T_e} \right), \quad (30)$$

where $X(Z, N)$ is the mass fraction of the nuclear species with Z protons and N neutrons, $G(Z, N)$ is the partition function, ρ is density, N_A is Avagadro's number, k is the Boltzmann constant, $Q_n(N, Z)$ is the nuclear Q-value, and A_n and A_p are the neutron and proton atomic masses, respectively. In equation (30), ρ_{10} is the density in units of 10^{10} g cm^{-3}. In order to estimate the number density of alpha particles, we use a plasma temperature calculated from a given entropy and the fitted density function (eq. [26]) as discussed in the last section.

To zero order in the ratio $\lambda_{e+}/\lambda_{v_e}$, the electron fraction in the presence of an alpha-particle component is given by (see eq. [9])

$$Y_e \approx Y_{e_0} + X_\alpha(0.5 - Y_{e_0}) . \quad (31)$$

The magnitude of the "alpha effect" on Y_e is proportional to the number of alpha particles and also to the difference between Y_{e_0} and $\frac{1}{2}$. If there are equal numbers of neutrons and protons, then there is no change in the electron fraction due to alpha-particle formation. However, if the neutron-to-proton ratio is not unity, then the effect of alpha-particle formation will be to drive Y_e closer to $\frac{1}{2}$. The expression in equation (31) does not include the small effect of electron and positron capture during this period. These captures may be accounted for by including the terms to first order in the ratio $\lambda_{e+}/\lambda_{v_e}$:

$$Y_e \approx Y_{e_0}$$

$$+ Y_{e_0} \frac{\lambda_{e+}}{\lambda_{v_e}} \left[1 - \left(1 + \frac{\lambda_{e-}}{\lambda_{e+}} \right) \Big/ \left(1 + \frac{\lambda_{\bar{v}_e}}{\lambda_{v_{\bar{e}}}} \right) \right]$$

$$+ X_\alpha(0.5 - Y_{e_0})$$

$$+ Y_{e_0} \frac{X_\alpha}{2} \left(\frac{\lambda_{e+}}{\lambda_{v_e}} \right)$$

$$\times \left[\frac{\lambda_{e-}}{\lambda_{e+}} - 1 - \left(\frac{\lambda_{\bar{v}_e}}{\lambda_{v_e}} - 1 \right) \left(\frac{\lambda_{e-}/\lambda_{e+} + 1}{\lambda_{\bar{v}_e}/\lambda_{v_e} + 1} \right) \right] . \quad (32)$$

The second line in this expression is the correction to the "equilibrium" Y_e from electron and positron captures on free nucleons discussed in the last section. The last line in equation (32) contains an additional correction term for the "equilibrium" Y_e that is due to the electron and positron capture processes on free nucleons when alpha particles are present. These additional terms give a more complete description of the "equilibrium" Y_e when alpha particles are present. Figure 6 shows the value of Y_{e_0} and the value of the "equilibrium" Y_e as a function of time for our example outflow trajectory. At early time and high temperature, the influence of the electrons and positrons can be seen by the increase in the "equilibrium" Y_e over Y_{e_0}. The minimum in
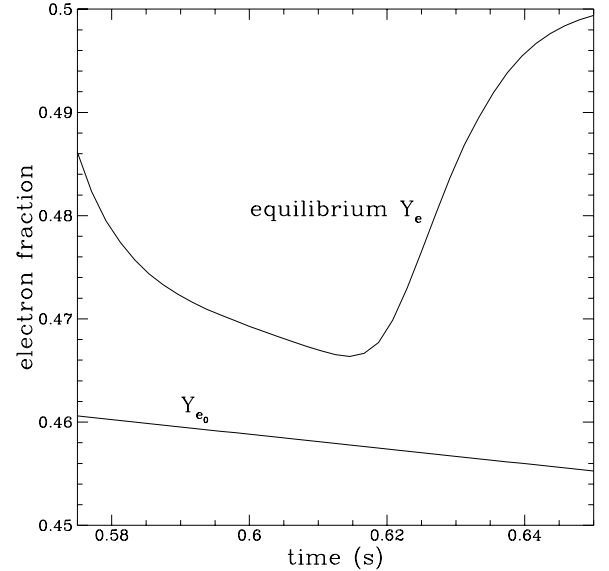

FIG. 6.—Value that the electron fraction would take if the system were in weak equilibrium. The lower curve takes into account only neutrino and antineutrino captures on free nucleons, as in Fig. 4. The upper curve takes into account electron and positron captures on free nucleons, as well as the incorporation of free nucleons into alpha particles.

the "equilibrium" Y_e curve occurs at the point at which alpha particles begin to form. The increase in "equilibrium" Y_e as time increases subsequent to the minimum is due to the "alpha effect." Since the true Y_e is not in equilibrium at the time of alpha-particle formation, the increase in the true Y_e will be much smaller than the increase in the "equilibrium" Y_e shown in the figure. The actual increase in the true Y_e depends on the rate of alpha-particle formation.

Since the process of incorporating nucleons into alpha particles is clearly an important factor for determining the electron fraction, we wish to explore the relationship between the rates of neutrino and antineutrino capture on free nucleons and the rate of alpha-particle formation. Assuming a *fast* and constant rate of alpha-particle formation $\dot{X}_\alpha = C_\alpha$, and assuming constant neutrino and antineutrino capture rates, we can integrate the differential equation for Y_e (eq. [9]) to obtain

$$Y_e \approx Y_{ei} + \frac{1}{2}(\lambda_{v_e} X_\alpha^2/C_\alpha)[1/(2Y_{e_0}) - 1] . \quad (33)$$

Here Y_{ei} is the value of the electron fraction before alpha-particle formation begins. Equation (33) will be valid during the epoch at which the alpha-particle abundance is changing and is accompanied by a continuously changing electron fraction. The presence of the term λ_{v_e}/C_α in equation (33) shows that there is a competition between alpha-particle formation and the neutrino capture on neutrons in setting Y_e. Either a faster neutrino capture rate or a slower rate of alpha-particle formation will result in an increased change in the electron fraction. If the material is neutron rich, this change will be positive. The last term in this expression shows that there will be little effect from alpha-particle formation when the electron fraction is close to $Y_e = 0.5$.

The change in the electron fraction due to alpha-particle formation may be estimated from equation (33). At $t_{\text{pb}} \approx 0.5$ s, the appropriate quantities taken from our calculations give $\lambda_{v_e}/C_\alpha \sim 5$ s^{-1}/50 s^{-1} ~ 0.1 and $[1/(2Y_{e_0}) - 1] \sim 0.3$.

Therefore, the change in the electron fraction as computed from equation (33) will be ~ 0.002, approximately 1%. The nonequilibrium calculation presented in § 6 gives the results of a more exact and detailed treatment of these issues. These results can be used to estimate how much different Y_e would be for different models of thermodynamic history and (anti)neutrino energy spectra.

6. NONEQUILIBRIUM CALCULATIONS

In this section we focus on the nonequilibrium aspect of the calculation of the electron fraction. In the previous sections we have focused on the " equilibrium " Y_e in order to show the general trends caused by each of the variables that influence the electron fraction. However, the relative magnitudes and effects of these factors can be determined definitively only by a full nonequilibrium calculation.

For this calculation, we employ an NSE computer code to keep track of thermodynamic variables, weak reaction rates, and the electron fraction in a representative mass element of outflowing material. As input, the code utilizes the density fit from equation (26), an assumed initial electron fraction, and a constant entropy as before. The outflow velocity of the material is obtained by interpolating with cubic splines between the velocity given in a particular run of the Wilson and Mayle results at different time slices. Other thermodynamic variables, such as temperature and chemical potential, are calculated self-consistently from these parameters as outlined in § 3 but are now modified where appropriate to include the effects of heavy nuclei. We calculate the relative abundances of free nucleons, alpha particles, and heavy nuclei from the thermodynamic variables and the current value of the electron fraction. The electron fraction is updated at each time step in our calculation by following all the charged current weak reaction rates.

During the periods when only free nucleons are present, the electron fraction determines the values of X_p and X_n. After alpha particles form, relative abundances are calculated with the electron fraction and the nuclear Saha equation for alpha particles, equation (30). During the periods when heavy nuclei are present, we use the liquid drop model and the prescription of Fuller (1982), Bethe et al. (1979, hereafter BBAL), Baym, Bethe, & Pethick (1971), and Lamb et al. (1978) to calculate the neutron and proton chemical potentials. In this model, the total energy of the nucleus with mass number A can be approximated as

$$W_N \approx W_{\text{bulk}} + W_{\text{surf}} A^{2/3} + W_{\text{coul}} A^{5/3} \ . \tag{34}$$

In this expression, W_{bulk} is the energy of bulk nuclear matter, while W_{surf} and W_{coul} are the coefficients of the surface energy and coulomb energy terms, respectively. The values for these coefficients given in BBAL and employed by Fuller (1982) are

$$W_{\text{surf}} \approx 290(Z/A)^2(1 - Z/A)^2 \ , \tag{35}$$

$$W_{\text{coul}} \approx 0.75(Z/A)^2(1 - 0.236\rho_{12}^{1/3} + 0.00194\rho_{12}) \ , \tag{36}$$

where ρ_{12} is the density in units of 10^{12} g cm^{-3} and Z is the number of protons in the nucleus. The value of the mean nuclear mass in NSE is obtained by minimizing W_N, which yields the condition that the nuclear surface energy should be twice the coulomb energy, from which we derive

$$A \approx 194[1 - (Z/A)]^2(1 - 0.236\rho_{12}^{1/3})^{-1} \ . \tag{37}$$

The difference in neutron and proton chemical potentials is given by

$$\hat{\mu} = \mu_n - \mu_p \approx 250 \left[0.5 - \left(\frac{Z}{A} \right) \right]$$
$$- W_{\text{surf}} A^{-1/3} \left\{ \frac{3 - 5(Z/A)}{(Z/A)[1 - (Z/A)]} \right\} \ . \tag{38}$$

The neutron chemical potential in this scheme is (Fuller 1982; BBAL)

$$\mu_n \approx -16 + 125 \left[0.5 - \left(\frac{Z}{A} \right) \right]$$
$$- 125 \left[0.5 - \left(\frac{Z}{A} \right) \right]^2 - \frac{W_{\text{surf}}}{A^{1/3}} \frac{3 - 7(Z/A)}{2[1 - (Z/A)]} \ . \tag{39}$$

For a recent calculation and discussion of the nuclear equation of state, see Lattimer & Swesty (1991).

The neutron chemical potential has the same value for the neutrons inside the nucleus and the neutrons in the free neutron gas. In the dilute Maxwell-Boltzmann limit that obtains for free nucleons, the mass fraction of free neutrons will be

$$X_n \approx 79 \frac{(T/\text{MeV})^{3/2}}{\rho_{10}} \exp \left(\frac{\mu_n}{T_e} \right), \tag{40}$$

while the corresponding mass fraction for free protons will be

$$X_p \approx X_n \exp \left(-\hat{\mu}/T_e \right) . \tag{41}$$

The mass fractions of heavy nuclei are calculated by using the nuclear Saha equation. The partition functions and binding energies employed in this prescription were taken from Woosley et al. (1978). Only heavy nuclei that contribute more than a few percent to the total heavy nucleus mass fraction at a given time are retained, and the abundance distribution is normalized to ensure that

$$X_p + X_n + X_\alpha + \sum_h X_h = 1 \ . \tag{42}$$

We allow the electron fraction to change by calculating weak capture rates on free nucleons and heavy nuclei. In the case of (anti)neutrino capture on free nucleons, the neutrino distribution functions (smoothed with time) are employed as discussed in § 3. The electron and positron capture rates are calculated for arbitrary degeneracy and without making any approximations in the lepton kinematics:

$$\lambda_{e^-} \approx (6.295 \times 10^{-4} \text{ s}^{-1}) \left(\frac{T_e}{m_e} \right)^5$$
$$\times \int_{E_{\text{TH}}^-}^\infty \frac{(x + Q_{e^-}/T_e)^2 x [x^2 - (m_e/T_e)^2]^{1/2}}{\exp (x - \mu_{e^-}/T_e) + 1} \, dx \ , \tag{43}$$

$$\lambda_{e^+} \approx (6.295 \times 10^{-4} \text{ s}^{-1}) \left(\frac{T_e}{m_e} \right)^5$$
$$\times \int_{E_{\text{TH}}^+}^\infty \frac{(x + Q_{e^+}/T_e)^2 x [x^2 - (m_e/T_e)^2]^{1/2}}{\exp (x - \mu_{e^+}/T_e) + 1} \, dx \ . \tag{44}$$

Here the Q-values and the energy thresholds are $Q_{e^+} \approx 1.293$ MeV and $E_{\text{TH}}^+ = m_e$ for positron capture on neutrons and $Q_{e^-} \approx -1.293$ MeV and $E_{\text{TH}}^- = m_n - m_p - m_e$ for electron capture on protons. In electromagnetic equilibrium, the sum of the total (kinetic plus rest mass) electron and

positron chemical potentials is zero, which implies that

$$\mu_{e+} = -\mu_{e-} \, . \tag{45}$$

We have included neutrino and antineutrino captures on heavy nuclei, calculated by the prescription given in Fuller & Meyer (1995) and McLaughlin & Fuller (1995). In these calculations, we employed Fermi-Dirac distribution functions for the neutrinos and antineutrinos normalized by the appropriate average energy and luminosity. The neutrino and antineutrino energy luminosities and average energies were taken from the Wilson and Mayle output at the relevant time slices. The average neutrino and antineutrino energies were fitted with straight lines, while the corresponding values for the luminosities were obtained using cubic spline interpolation.

We start our calculations in conditions in which weak equilibrium obtains, so that we can employ the solution to equation (11) as an initial electron fraction. We hold the entropy constant throughout our calculation, since we are far from the gain radius when the calculation begins. The adiabatic outflow approximation is employed here in keeping with our spirit of discerning the basic physics important for Y_e. We would expect the entropy of an actual outflowing mass element to rise moderately through the regime of weak freezeout (see Qian & Woosley 1996). The resulting "nonequilibrium" electron fraction for three different constant entropy trajectories is shown in Figure 7. The resulting electron fraction for all the curves follows a downward trend at the earliest times. This trend corresponds to the effect of the decreasing importance of the electron and positron capture rates, as discussed in § 3. The curve with the highest entropy begins with highest electron temperature, since the density history is the same for all of these curves. This also explains the increase in the electron fraction with increasing entropy, since the plasma temperature and, hence, the effect of electron and positron capture will be larger at higher entropy. The dip in these curves occurs when alpha particles begin to form. This is a smaller version of the effect in the "equilibrium" case which was discussed in § 5. It can be seen that the smallest "alpha effect" occurs for the case where the electron fraction is closest to $\frac{1}{2}$.
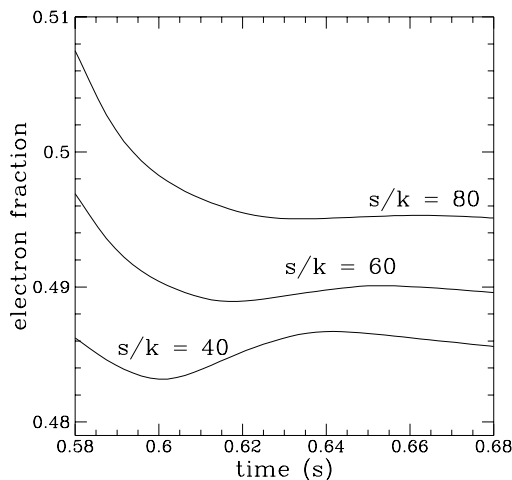

Fig. 7.—Value of the electron fraction derived from a nonequilibrium calculation. The entropy was held constant as the mass element flowed away from the neutron star. Three different curves are shown, each with a different value for the entropy, as indicated.
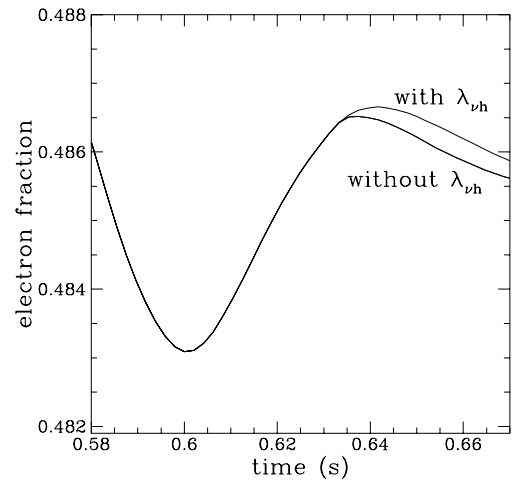

Fig. 8.—Results of a nonequilibrium calculation for the electron fraction are shown in which neutrino and antineutrino captures on heavy nuclei are included (upper curve) and not included (lower curve). The electron fraction is plotted against time post–core bounce.

In this graph, heavy nuclei form starting at an epoch between $t_{pb} \approx 0.64$ s and $t_{pb} \approx 0.66$ s. After the heavy nuclei form, the system contains mostly heavy nuclei with a few percent of the mass fraction in protons. Protons are capturing antineutrinos, and this tends to decrease the electron fraction. However, counteracting this effect are neutrino captures on heavy nuclei, which tend to increase the electron fraction. The result is the almost flat curves seen at late time in Figure 7. Figure 8 further demonstrates the effect of neutrino and antineutrino capture on heavy nuclei for a trajectory with entropy $s/k \approx 40$. This figure shows the Y_e that is obtained when captures on heavy nuclei are included (upper curve) and are not included (lower curve) in the calculation. The captures on heavy nuclei represent a relatively small effect, which does not affect the resulting electron fraction by more than 1%.

We find that the value of the electron fraction is close to Y_{eo} throughout the time period when the system is falling out of weak equilibrium. Although the formation of alpha particles, neutrino and antineutrino capture on heavy nuclei, and electron (positron) capture on free nucleons can have significant leverage on the final electron fraction, the ratio of the antineutrino to neutrino capture rate on free nucleons at the time of freezeout from weak equilibrium has the most influence. However, the relative leverage on Y_e of the effects considered here can vary with different outflow conditions.

7. CONCLUSION

In this paper we have given an in-depth treatment and analysis of the evolution of the electron fraction in neutrino-heated supernova outflow, including detailed treatment of the effects of nuclear composition changes. Our study has concentrated on the time $t_{pb} \lesssim 1$ s. The evolution of Y_e is this epoch may be quite important for models of the light p-process and the neutron number $N \approx 50$ r-process nuclei (Hoffman et al. 1996a; Fuller & Meyer 1995).

We have employed fits to the detailed neutrino and antineutrino energy spectra from the Wilson and Mayle supernova calculations. We find that these detailed spectra are necessary for computations of weak rates to the level of accuracy in Y_e that may be required for nucleosynthesis

considerations. However, we find that hydrodynamic wave-induced fluctuations in the ratios of neutrino and antineutrino spectral parameters with time produce significant excursions in Y_e. We find that the rates of electron and positron capture on free nucleons can also be important for computing the evolution of the electron fraction. The charged current weak rates freeze out from equilibrium at a time when the electron and positron capture rates may still have some influence on Y_e. During this time period, the effect of these rates is to increase the electron fraction. We have given detailed calculations of the "alpha effect"—the increase in the electron fraction caused by a changing alpha-particle mass fraction. Our results indicate that the alpha effect can play a very significant role in setting Y_e.

We have employed numerical calculations of nuclear composition changes in nuclear statistical equilibrium, coupled with fits to density and velocity of outflow histories from the Wilson and Mayle results, to compute the evolution of Y_e. These calculations explicitly include all charged current weak interaction processes, including neutrino and antineutrino capture on heavy nuclei. We follow the evolution of Y_e through the epoch of weak equilibrium freezeout. These calculations show that the combination of neutrino and antineutrino capture on heavy nuclei and antineutrino capture on free protons tends to keep Y_e constant. The results presented in this paper are meant to illustrate several different variables and processes that can alter the electron fraction in post–core bounce supernova outflow. Clearly, more sophisticated models of neutrino transport and hydrodynamic outflow than those employed here would be necessary to actually *predict* Y_e in a reliable fashion. We believe, however, that the effects described here will always play the major role in setting Y_e.

REFERENCES

Bethe, H. A., & Wilson, J. R. 1985, ApJ, 263, 386
Baym, G., Bethe, H. A., & Pethick, C. 1971, Nucl. Phys., A175, 225
Bethe, H. A., Browne, G. E., Applegate J., & Lattimer, J. M. 1979, Nucl. Phys., A324, 487 (BBAL)
Burrows, A., Hayes, J., & Fryxell, B. A. 1995, ApJ 450, 830
Caldwell, D., Fuller, G. M., & Qian, Y.-Z. 1996, in preparation
Duncan, R. C., Shapiro, S. L., & Wasserman, I. 1986, ApJ, 309, 141
Fuller, G. M. 1982, ApJ, 252, 741
———. 1993, Phys. Rep., 227, 149
Fuller, G. M., Fowler, W. A., & Newman, M. J. 1980, ApJS, 42, 447
———. 1982a, ApJ, 252, 715
———. 1982b, ApJS, 48, 279
———. 1985, ApJ, 293, 1
Fuller, G. M., Mayle, R., Meyer, B. S., & Wilson, J. R. 1992, ApJ, 389, 517
Fuller, G. M., & Meyer, B. S. 1995, ApJ, 453, 792; erratum 1996, ApJ, 464, 521
Fuller, G. M., Qian, Y.-Z., & Wilson, J. R. 1996, in preparation
Herant, M., Benz, W., Hix, W. R., Fryer, C. L., & Colgate, S. A. 1994, ApJ, 435, 339
Hoffman, R. D., Woosley, S. E., Fuller, G. M., & Meyer, B. S. 1996a, ApJ, 460, 478
Hoffman, R. D., Woosley, S. E., Qian, Y.-Z., & Fuller, G. M. 1996b, in preparation

Janka, H.-T., & Müller, E. 1995, ApJ, 448, L109
———. 1996, A&A, 306, 167
Lamb, D. Q., Lattimer, J. M., Pethick, C. J., & Ravenhall, D. G. 1978, Phys. Rev. Lett., 41, 1623
Lattimer, J. M., & Swesty, F. D. 1991, Nucl. Phys., A535, 331
McLaughlin, G. C., & Fuller, G. M. 1995, ApJ, 455, 202; erratum 1996, ApJ, 466, 1100
Meyer, B. S. 1995, ApJ, 455, L55
Meyer, B. S., Brown, J. S., & Luo, N. 1996, preprint
Meyer, B. S., Howard, W. M., Matthews, G. J., Woosley, S. E., & Hoffman, R. D. 1992, ApJ, 399, 656
Miller, D. S., Wilson, J. R., & Mayle, R. W. 1993, ApJ, 415, 278
Qian, Y.-Z. 1993, Ph.D. thesis, Univ. of California, San Diego,
Qian, Y.-Z., & Fuller, G. M. 1995, Phys. Rev. D, 52, 656
Qian, Y.-Z., Fuller, G. M., Mathews, G. J., Mayle, R. W., Wilson, J. R., & Woosley, S. E. 1993, Phys. Rev. Lett., 71, 1965
Qian, Y.-Z., & Woosley, S. E. 1996, ApJ, in press
Witti, J., Janka, H.-T., & Takahashi, K. 1994, A&A, 286, 841
Woosley, S. E., & Baron, E. 1992, ApJ, 391, 228
Woosley, S. E., Fowler, W. A., Holmes, J. A., & Zimmerman, B. A. 1978, Atomic Data Nucl. Data Tables, 23, 371
Woosley, S. E., et al. 1994, ApJ, 443, 229
Woosley, S. E., & Hoffman, R. D. 1992, ApJ, 395, 202